



# Bayesian estimation of Earth's climate sensitivity and transient climate response from observational warming and heat content datasets

5 Philip Goodwin<sup>1</sup>, B. B. Cael<sup>2</sup>

<sup>1</sup>School of Ocean and Earth Science, University of Southampton, SO13 3ZH, UK

<sup>2</sup>National Oceanography Centre, Southampton, SO13 3ZH, UK

*Correspondence to:* Philip Goodwin (p.a.goodwin@soton.ac.uk)

10 **Abstract.** Future climate change projections, impacts and mitigation targets are directly affected by how sensitive Earth's  
global mean surface temperature is to anthropogenic forcing, expressed via the effective climate sensitivity (ECS) and  
transient climate response (TCR). However, the ECS and TCR are poorly constrained, in part because historic observations  
and future climate projections consider the climate system under different response timescales with potentially different  
climate feedback strengths. Here, we evaluate ECS and TCR by using historic observations of surface warming, since the  
15 mid-19<sup>th</sup> century, and ocean heat uptake, since the mid 20<sup>th</sup> century, to constrain a model with independent climate feedback  
components acting over multiple response timescales. Adopting a Bayesian approach, our prior uses a constrained  
distribution for the instantaneous Planck feedback combined with wide-ranging uniform distributions of the strengths of the  
fast feedbacks (acting over several days) and slow feedbacks (acting over decades). We extract posterior distributions by  
applying likelihood functions derived from different combinations of observational datasets. The resulting TCR distributions  
20 are similar when using different historic datasets: from a TCR of 1.5 (1.3 to 1.7 at 5-95% range) °C, up to 1.7 (1.4 to 2.0) °C.  
However, the posterior probability distribution for ECS on a 100-year response timescale varies depending on which  
combinations of temperature and heat content anomaly datasets are used: from ECS of 2.2 (1.5 to 4.5) °C, for datasets with  
less historic warming, up to 2.8 (1.8 to 6.1) °C, for datasets with more historic warming. Our results demonstrate how  
differences between historic climate reconstructions imply significant differences in expected future global warming.

## 25 1 Introduction

A key goal in climate science is to evaluate how sensitive global mean temperature anomaly is to radiative forcing from  
greenhouse gasses and aerosols (e.g. Knutti et al., 2017; IPCC, 2013). This sensitivity of climate may be explored by  
considering how a global surface temperature anomaly affects Earth's radiation balance. The effective climate feedback,  
 $\lambda_{eff}$  ( $\text{Wm}^{-2}\text{K}^{-1}$ ), expresses the how surface warming increases outgoing radiation at the top of the atmosphere.  $\lambda_{eff}$  at some  
30 time  $t$  is calculated from the total radiative forcing,  $R_{total}$  ( $\text{Wm}^{-2}$ ), the net top-of-atmosphere energy imbalance,  $N$  ( $\text{Wm}^{-2}$ ),  
and the global surface temperature anomaly,  $\Delta T$  (K), via



$$\lambda_{eff}(t) = (R_{total}(t) - N(t))/\Delta T(t) \quad (1)$$

35 where both  $R_{total}$  and  $\Delta T$  are defined as zero at some preindustrial state. The Effective Climate Sensitivity at some time  $t$ , ECS( $t$ ) in K, is then defined as the radiative forcing for a doubling of CO<sub>2</sub>,  $R_{2\times CO_2}$ , divided by  $\lambda_{eff}(t)$ ,

$$ECS(t) = \frac{R_{2\times CO_2}}{\lambda_{eff}(t)} = \frac{R_{2\times CO_2}\Delta T(t)}{R_{total}(t) - N(t)} \quad (2)$$

40 ECS and  $\lambda_{eff}$  may be evaluated from estimates of historic radiative forcing and observational constraints on  $\Delta T$  and  $N$ , eqns. (1, 2); noting that Earth's energy imbalance,  $N$ , can be observationally constrained as a time-average through reconstructing the heat content changes in the Earth system dominated by the ocean (e.g. Cheng et al., 2017; Levitus et al., 2012).

Many previous studies evaluating ECS from historical observational data and radiative forcing estimates, eq. (2), have either  
45 calculated a single constant climate sensitivity (see Annan, 2015; Anan and Hargreaves, 2020; Bodman and Jones, 2016; Lewis and Curry, 2014; Sherwood et al., 2020; Skeie et al., 2018; Otto et al., 2013), or have evaluated ECS for specific historic periods (e.g. Tokarska et al., 2020), acknowledging that the value for the specific historical period may not apply for all timescales into the future.

50 The assumption of a single constant ECS over time leads to uncertainties arising from model inadequacy (Annan, 2015), since climate sensitivity may not be constant with time or across different response timescales (e.g. Rugenstein et al., 2020; Rohling et al., 2012; 2018; Goodwin, 2018; Knutti et al., 2017; Senior and Mitchell, 2000; Proistosescu and Huybers, 2017). There is also the possibility that, at any given time or timescale, the climate feedback may be different for different sources of radiative forcing, such as well mixed greenhouse gasses and volcanic aerosols (e.g. Marvel et al., 2015).

55 The aim here is to perform Bayesian probabilistic evaluations of both ECS and transient climate response (TCR in K), using observational constraints on global surface temperature and ocean heat content anomalies to constrain a model framework that includes time-varying climate feedbacks, eqns. (1, 2). Our estimates are independent of simulated warming responses in complex climate models.

60 We utilise a numerical model where multiple climate feedbacks each respond to radiative forcing over different timescales (Goodwin, 2018), allowing  $\lambda_{eff}$  to vary over time (eqns. 1,2). Generating a prior model ensemble with varying fast and slow climate feedback strengths, we extract four posterior ensembles using a Bayesian comparison to observational



reconstructions. Each posterior ensemble applies a different combination of historic reconstructions of global surface  
65 temperature anomaly (either HadCRUT4: Morice et al., 2012; or Cowtan&Way version 2.0 ‘HadCRUT4 infilled by kriging’:  
Cowtan & Way, 2014) and reconstruction of ocean heat content anomaly (either NODC: Levitus et al., 2012; or Cheng et al:  
Cheng et al., 2017). All our posterior ensembles are extracted using the additional constraints from HadSST3.1 (Kennedy et  
al., 2011) and Global Carbon Budget (le Quéré et al., 2018) for sea surface temperature and ocean carbon uptake anomalies  
respectively.

## 70 **2 Model of surface warming from time-varying climate feedback**

Quisque Equation (1) considers surface warming via a single effective climate feedback response to total radiative forcing,  
where the effective climate feedback represents an aggregated response to multiple climate feedbacks to multiple sources of  
radiative forcing. Here, surface warming is modelled as an extended energy balance response to  $i$  sources of radiative forcing  
by  $j$  climate feedbacks operating over different response timescales (Goodwin, 2018),

75

$$\Delta T(t) = \left(1 - \frac{N(t)}{R_{total}(t)}\right) \sum_i \left[ \frac{R_i(t)}{\lambda_{planck} + \sum_j \lambda_{i,j}(t)} \right] \quad (3)$$

The  $j$  combinations of climate feedbacks processes considered here are:

- 80 (1)  $\lambda_{fast}$ , the combined fast feedbacks operating over response timescales approximately linked to the residence timescale of  
water vapour in the atmosphere (van der Ent and Tuinenberg, 2017), including clouds, water vapour-lapse rate, snow and  
sea-ice surface albedo; and  
(2)  $\lambda_{slow}$ , the combined slow feedbacks operating over a multi-decadal timescale that may, for example, be linked to a  
surface warming pattern adjustment (e.g. Andrews et al., 2015).

85 The  $i$  sources of radiative forcing used in eq. (3) are:

- (1) Atmospheric CO<sub>2</sub> forcing, calculated from CO<sub>2</sub> concentrations using  $R_{CO_2} = a_{CO_2} \Delta \ln CO_2$  after IPCC (2013);  
(2) Combined forcing from other well mixed greenhouse gases,  $R_{WMGHG}$ , including methane, nitrous oxides each calculated  
from concentrations after Etminan et al. (2016) (see Supplementary Information), and Halocarbons after IPCC (2013);  
(3) Combined direct and indirect anthropogenic aerosol forcing, linked annual aerosol emission rates (Myhre et al., 2013;  
90 Smith et al., 2018, see Supplementary Information);  
(4) Volcanic aerosol radiative forcing, calculated after 1850 from volcanic Aerosol Optical Depth (AOD) using  $R_{volcanic} =$   
 $-(19 \pm 0.5)AOD$  (Gregory et al., 2016) and before 1850 from the global radiative forcing timeseries used in the Reduced  
Complexity Model Intercomparison Project (RCMIP) phase 1 (Nicholls et al., 2020 in press), with identical relative  
uncertainty imposed both pre and post 1850;  
95 (5) Solar forcing; and



(6) Internal variability in Earth's energy imbalance, imposed using AR1 noise with coefficients chosen to approximate the properties of monthly and yearly average noise from Trenberth et al. (2014).

When radiative forcing from source  $i$  is not increasing in magnitude between times  $t$  and  $t + \delta t$ ,  $|R_i(t + \delta t)| \leq |R_i(t)|$ , the  
100  $j$ th combination of climate feedback processes evolves according to,

$$\lambda_{i,j}(t + \delta t) = \lambda_{i,j}(t) + \left(\lambda_j^{equil} - \lambda_{i,j}(t)\right) \left(1 - \exp\left(\frac{-\delta t}{\tau_j}\right)\right) \quad (4)$$

However, when radiative forcing from source  $i$  is increasing in magnitude,  $|R_i(t + \delta t)| > |R_i(t)|$ , climate feedback  $\lambda_{i,j}$   
105 evolves from  $t$  to  $t + \delta t$  according to,

$$\lambda_{i,j}(t + \delta t) = \left|\frac{R_i(t)}{R_i(t + \delta t)}\right| \left(\lambda_{i,j}(t) + \left(\lambda_j^{equil} - \lambda_{i,j}(t)\right) \left(1 - \exp\left(\frac{-\delta t}{\tau_j}\right)\right)\right) \quad (5)$$

Thus, from eqns. (3), (4) and (5), any additional radiative forcing acts instantaneously at the Planck feedback in the first  
110 time-step it is applied, and then evolves over the e-folding response timescales  $\tau_j$  towards the equilibrium climate feedback,  
 $\lambda_{equilibrium} = \lambda_{planck} + \lambda_{fast}^{equil} + \lambda_{slow}^{equil}$ . Since (5) is applied separately for each of the  $j$  sources of radiative forcing, the  
framework used here allows different values of climate feedback at any point in time for each source of radiative forcing.

This model of climate feedbacks responding to imposed radiative forcing over multiple response timescales, eqns. (3), (4)  
115 and (5), produces a time-evolving effective climate feedback, (1), and time-evolving Effective Climate Sensitivity, (2), in  
response to a prescribed forcing scenario. Here, the transient climate response, TCR, is calculated as the 11-year average  
warming centred at the year of CO<sub>2</sub> doubling for a scenario with a 1 per cent per year rise in CO<sub>2</sub> and no other forcing  
(hereafter: 1pctCO<sub>2</sub> scenario).

### 120 3 Generation of the prior and posterior ensembles

We generate probabilistic prior and posterior model ensembles with varied model input parameters using Bayes' theorem.  
The joint posterior probability that the climate system parameters  $X$  have a specific set of values  $X'$  given background  
information  $I$  and observations of the climate system  $\{obs\}$ ,  $prob(X = X'|\{obs\}, I)$ , is expressed using Bayes' theorem,

125



$$prob(X = X'|\{obs\}, I) \propto prob(\{obs\}|X = X', I) \times prob(X = X'|I) \quad (6)$$

where:

- (1)  $prob(X = X'|I)$  is the joint prior probability that  $X = X'$  for climate system parameter values (Supplementary Table S1; Fig. 2 solid lines for  $\lambda_{Planck}$ ,  $\lambda_{Fast}^{equil}$  and  $\lambda_{Slow}^{equil}$ ); and
- (2)  $prob(\{obs\}|X = X', I)$  is known as the likelihood function and expresses the probability of obtaining the observations in  $\{obs\}$  for the given joint parameter values  $X = X'$  and background information  $I$ . Here, this is estimated from where the simulated model observables for  $X = X'$  and  $I$  lie on the probability distributions for the real observables (Supplementary Table S2).

135

Here, we use large ensemble simulations of the Warming Acidification and Sea level Projector (WASP) model (Goodwin, 2016), adopting the updated version of Goodwin (2018) with explicitly time-evolving climate feedbacks (eqns. 3, 4 and 5). This version of WASP does not contain a single parameter for ECS or  $\lambda_{eff}$  at some time  $t$ , eqns. (1, 2). Instead, the values of ECS and  $\lambda_{eff}$  emerge over time in the model in response to the forcing scenario from a combination of multiple prescribed climate system parameters (eqns. 3, 4, 5). The WASP model contains a 5-box representation of ocean heat and carbon uptake, with an ocean circulation that is varied between ensemble members but remains constant in time within each ensemble member (Supplementary Table S1).

We form a prior model ensemble where a total of 25 model input parameters independently varied between simulations (Supplementary Table S1), to represent the prior climate system parameter distribution  $X$ , eq. (6). Five of the input parameters within  $X$  describe how climate feedback responds to an imposed radiative forcing ( $\lambda_{Planck}$ ,  $\lambda_{fast}^{equil}$ ,  $\lambda_{slow}^{equil}$ ,  $\tau_{Fast}$  and  $\tau_{Slow}$ ) with a 6<sup>th</sup> input parameter (the radiative forcing coefficient for CO<sub>2</sub>) converting this climate feedback to Effective Climate Sensitivity (Supplementary Table S1, eq. 2).

A further thirteen of the 25 model input parameters varied within  $X$  relate to uncertainty in historic radiative forcing (Supplementary Table S1). The WASP model is historically forced until 2014 (following the ssp585 scenario thereafter: O'Neill et al., 2016) with atmospheric concentrations of greenhouse gasses; direct and indirect radiative forcing from anthropogenic aerosols; radiative forcing from volcanic aerosols; and solar forcing (see Supplementary Information). The radiative forcing from each component (aside from solar forcing) is varied between simulations in the prior ensemble (Supplementary Table S1) to approximate historic uncertainty (Myhre et al., 2013; Etminan et al., 2016; Smith et al., 2018; Gregory et al., 2016).

155



Normal input distributions (Supplementary Table S1) are used to represent historic uncertainty in: the radiative forcing sensitivity to greenhouse gas concentrations (Myhre et al., 2013; Etminan et al., 2016); the direct radiative forcing sensitivity to anthropogenic aerosol emissions for six separate aerosol types (Myhre et al., 2013), and the radiative forcing sensitivity to volcanic aerosol optical depth (Gregory et al., 2016). However, a skew-normal input distribution is used to represent historic uncertainty in the indirect radiative forcing from anthropogenic aerosols (Supplementary Table S1), since there is a long tail of possibly strong-negative radiative forcing from this effect (IPCC, 2013).

We generate prior ensembles containing  $6.825 \times 10^8$  ensemble members, with the 25 input parameters independently varied such that the relative frequency distributions of each input parameter are set to the assumed prior probability distribution,  $prob(X = X'|I)$  in eq. (6) (Supplementary Table S1; Fig. 2 solid lines for  $\lambda_{Planck}$ ,  $\lambda_{Fast}^{equil}$  and  $\lambda_{Slow}^{equil}$ ). Observational tests are then used to form a likelihood function and extract a subset of the prior ensemble simulations into the posterior ensembles (Supplementary Table S2).

There are  $n = 12$  observational constraints within  $\{obs\}$  (Supplementary Table S2). The probability of obtaining the  $k^{th}$  observational constraint given  $X = X'$  and  $I$  is calculated assuming Gaussian uncertainty in the observable (e.g. Annan and Hargreaves, 2020),

$$prob(\{obs\}_k | X = X', I) \propto e^{-\frac{(\mu_k - x_k)^2}{2\sigma_k^2}} \quad (7)$$

where  $\mu_k$  and  $\sigma_k$  are the observational mean and standard deviation uncertainty of observable  $k$  (Supplementary Table 2), and  $x_k$  is the simulated value of the observable for  $X = X'$  and  $I$ . To calculate the overall probability of obtaining all  $n$  observational constraints within  $\{obs\}$  given  $X = X'$  and  $I$ , we multiply the probabilities for all  $\{obs\}_k$ ,

$$prob(\{obs\} | X = X', I) = \prod_{k=1}^n prob(\{obs\}_k | X = X', I) \quad (8)$$

Four different ensembles are generated using different combinations of surface temperature (HadCRUT4 and Cowtan&Way; Fig. 1a) and heat content (NODC and Cheng et al.; Fig. 1b) datasets to construct the likelihood function that acts as a constraint on the posterior (eq. 6). These model ensembles are termed HadCRUT4 + NODC; HadCRUT4 + Cheng et al.; Cowtan&Way + NODC; and Cowtan&Way + Cheng et al. (Supplementary Table S2). For each of these four ensembles, the probability of a prior simulation being included within the posterior ensemble is proportional to  $prob(\{obs\} | X = X', I)$ , eqn. (8): a simulation is accepted into the posterior ensemble if the value of  $prob(\{obs\} | X = X', I)$ , assessed using (8), is greater than a number randomly drawn between 0 and some number greater than the maximum value of  $prob(\{obs\} | X = X', I)$  achieved in that prior ensemble.



190 We adopt a normal prior distribution for  $\lambda_{Planck}$ , informed by Earth's global mean surface temperature (Jones and Harpham,  
2013) and radiation budget (Trenberth et al., 2014) (Fig. 2, solid black line). We adopt uniform prior distributions of  $\lambda_{Fast}^{equil}$   
and  $\lambda_{Slow}^{equil}$  (Fig. 2, solid blue and red lines), thus assuming that any value within the boundaries is equally likely before we  
consider the observations,  $\{obs\}$  (eq. 6). Our boundaries for the uniform distributions of  $\lambda_{Fast}^{equil}$  and  $\lambda_{Slow}^{equil}$  are set wide  
195 enough such that the posterior distributions are not significantly affected by the boundaries (Fig. 2, red and blue), but narrow  
enough such that the problem is computationally tractable.

#### 4 Results

In From the initial  $6.825 \times 10^8$  simulations in each prior ensemble, a total of 23804 simulations are accepted into the  
HadCRUT4 + NODC posterior ensemble; 10681 into the HadCRUT4 + Cheng et al. posterior ensemble; 1561 into the  
Cowtan&Way + NODC posterior ensemble; and 781 into the Cowtan&Way + Cheng et al. posterior ensemble. Fewer  
200 simulations are accepted into the posterior ensembles that use likelihood function terms,  $prob(\{obs\}_k | X = X', I)$  in eq. (7),  
with smaller observational uncertainty,  $\sigma_k$  (Supplementary Table S2).

The posterior distributions reveal both the Planck feedback and fast feedback strengths are insensitive to the combination of  
temperature and heat content datasets used within the likelihood function:  $\lambda_{Planck} = 3.2 \pm 0.1 \text{ Wm}^{-2}\text{K}^{-1}$  for all ensembles  
205 (mean  $\pm$  standard deviation), while  $\lambda_{Fast}^{equil} = -1.2 \pm 0.6 \text{ Wm}^{-2}\text{K}^{-1}$  for the HadCRUT4 + NODC ensemble and  $\lambda_{Fast}^{equil} =$   
 $-1.2 \pm 0.5 \text{ Wm}^{-2}\text{K}^{-1}$  for the other three ensembles. However, the different combinations of warming and heat content  
datasets used in the likelihood function result in different distributions for the slow feedback strengths.

For ensembles constrained by HadCRUT4 the slow feedback strength distributions have larger variance and less negative  
210 means:  $\lambda_{Slow}^{equil} = -0.4 \pm 1.0 \text{ Wm}^{-2}\text{K}^{-1}$  and  $\lambda_{Slow}^{equil} = -0.4 \pm 0.9 \text{ Wm}^{-2}\text{K}^{-1}$  when HadCRUT4 is combined with NODC and  
Cheng et al. respectively. When Cowtan&Way is used to constrain temperature, the slow feedback strength distributions  
have smaller variance and more negative means:  $\lambda_{Slow}^{equil} = -0.7 \pm 0.8 \text{ Wm}^{-2}\text{K}^{-1}$  and  $\lambda_{Slow}^{equil} = -0.8 \pm 0.8 \text{ Wm}^{-2}\text{K}^{-1}$  when  
Cowtan&Way is combined with NODC and Cheng et al. respectively. Noting that the sign convention is such that negative  
 $\lambda_{Slow}^{equil}$  values contribute more positive climate feedback, the interpretation considered here is that the increased recent  
215 warming in Cowtan&Way relative to HadCRUT4 (Fig. 1) implies that surface warming will receive more amplification, or  
less damping, from slow climate feedbacks into the future (Fig. 2, compare red dashed and dotted lines).



#### 4.1 The Effective Climate Sensitivity and Transient Climate Response

The ECS is analysed by forcing the four posterior ensembles with an instantaneous step-function quadrupling of atmospheric CO<sub>2</sub> (hereafter: 4xCO<sub>2</sub> scenario) and applying eq. (2). The value of ECS changes over time (Figs. 3,4) as the fast and slow climate feedbacks evolve in response to the imposed radiative forcing (eqns. 3, 4, 5).

For each combination of datasets used, the ECS is best constrained from the historic observational reconstructions on 20-year timescale (Figs. 3, 4a, Table 1). These 20-year response timescale ECS estimates are also similar between different datasets: varying from 2.0 °C (1.6 to 2.5 °C at 90% range) for the HadCRUT4 and NODC datasets to 2.2 °C (1.8 to 2.7 °C) for the Cowtan&Way and Cheng et al. dataset combination.

The distributions see a general increase in ECS out to 50-year and 100-year timescales, with greater uncertainty (Figs. 3,4) due to the uncertainty in how slow climate feedback will evolve (Fig. 2). The TCR is analysed by forcing our posterior ensembles with a scenario with a 1pctCO<sub>2</sub> scenario and recoding the surface warming for each ensemble member for the 11-year average centred on the year in which CO<sub>2</sub> reaches twice its initial value (Fig. 5).

#### 4.2 Variation in the posterior model ensembles

The observational records provide constraints on the parameters of the posterior ensembles that manifest not only as posterior distributions for these parameters but also as relationships between them, as well as between model parameters and key model outputs of interest (such as ECS(t)). While the correlation structure of the 25 parameters' joint posterior distribution is generally quite complex, some key structures emerge that indicate how ECS and TCR uncertainties might be reduced.

##### 4.2.1 Correlations of model parameters and outputs

We assemble the four observationally-consistent ensembles into a single meta-ensemble, where each model realization is weighted inversely to the number of members in its individual ensemble such that each of the four observational combinations is weighed equally (henceforth all analyses in this section are weighted, i.e. weighted correlations, weighted principal component analysis, and weighted stepwise regression). We then first examine the correlations between individual model parameters. Most notably, we find two strongly compensating pairs of model parameters. First,  $r_1$  (the ratio of global near-surface warming to global sea surface warming at equilibrium) and  $r_2$  (the ratio of global whole-ocean warming to global sea surface warming at equilibrium) strongly compensate ( $\rho = -0.83$ ), indicating the ratio of near-surface warming to global whole-ocean warming is tightly constrained by these datasets. Second,  $\lambda_{fast}^{equil}$  and  $\lambda_{slow}^{equil}$  are also strongly compensating ( $\rho = -0.89$ ). Neither of these are surprising as they reflect the primary constraints of the observations, i.e. ocean and near-surface warming histories, but the latter does indicate that a better-constrained fast feedback parameter  $\lambda_{fast}^{equil}$



250 would directly reduce uncertainty on  $\lambda_{slow}^{equil}$  and thereby ECS on multidecadal and centennial timescales. This is further corroborated by weaker but appreciable correlations between  $\lambda_{Plank}$  and  $\lambda_{fast}^{equil}$  ( $\rho = -0.46$ ) and  $\lambda_{slow}^{equil}$  ( $\rho = 0.37$ ).  $r_1$  also correlates appreciably with the timescale of upper ocean carbon exchange ( $\tau_{upper}$ ,  $\rho = 0.35$ ) and  $r_2$  also correlates appreciably with the CO<sub>2</sub> radiative forcing coefficient ( $a_{CO_2}$ ,  $\rho = 0.42$ ), while  $\lambda_{slow}^{equil}$  correlates appreciably with the aerosol-cloud interaction radiative forcing coefficient ( $R_{aci:2011}$ ) which in turn correlates appreciably with the SO<sub>x</sub> aerosol radiative forcing coefficient ( $\gamma_{aero-SO_x}$ ,  $\rho = 0.47$ ). Other correlations are significant due to the large meta-ensemble size but are not particularly strong ( $|\rho| < 0.28$ ) so are not mentioned here (note that this threshold and the 0.48 threshold below are arbitrarily chosen; in this section we are only interested in and therefore only report the strongest correlations).

Model outputs are in general correlated in expected fashions with each other and with model parameters. The time-average global mean  $\Delta T$ 's before 1940 are tightly correlated ( $\rho \in (0.60, 0.85)$ ), while the  $\Delta T$ 's on either side of the 1961-1990 reference temperature (1960-1979 vs. 1980-1999) strongly compensate ( $\rho = -0.92$ ); ocean heat content from 700-2000m is well-correlated with total ocean heat content ( $\rho = 0.64$ ). The ECS on a 50-year timescale, ECS<sub>50</sub>, is well correlated with ECS<sub>20</sub> ( $\rho = 0.50$ ) and especially with ECS<sub>100</sub> ( $\rho = 0.93$ ); we therefore focus on ECS<sub>20</sub> and ECS<sub>100</sub> hereafter. ECS<sub>100</sub> is correlated with  $\lambda_{slow}^{equil}$  ( $\rho = -0.56$ ), and ocean heat and carbon content are correlated with the upper ocean tracer exchange timescales and the warming ratios  $r_1$  and  $r_2$  ( $\rho \in (0.52, 0.63)$ ). 19th-century sea surface temperature anomaly is also strongly correlated with  $r_1$  (and hence strongly anticorrelated with  $r_2$ ). Other correlations between model outputs or between model outputs and parameters are significant due to the large meta-ensemble size but are weaker than the above ( $|\rho| < 0.48$ ) so are not discussed here.

#### 270 4.2.2 Principle components

Correlations between model parameters' posteriors imply that the dimensionality of the parameter space can be reduced and that the observational constraints collapse the posterior solution into a parameter space with fewer degrees of freedom. Principal Component Analysis, PCA (Jolliffe, 1986; n.b. we do not describe the method here as it is well-described in many textbooks such as Jolliffe, 1986) is a straightforward, ubiquitous means to identify these degrees of freedom, and is justifiable here in the absence of strongly nonlinear model equations and given the Gaussian or near-Gaussian likelihoods and priors. We perform a PCA on the model parameters' joint posterior; the results are presented in Figure 6. In the scree plot (fig. 6a) there is an obvious break point at the fifth principal component (PC), indicating the first four PCs are interpretable and the remaining are unstructured variations (Cattell, 1966). These PCs are shown in fig. 6b-e, with loadings of parameters grouped into feedbacks, oceanic parameters, aerosol sensitivities, and greenhouse gas sensitivities (we include the full PCs in the Supplemental Information (Supplementary Figures S1-S4) for completeness). The first three of these PCs are dominated by feedbacks, radiative forcing from aerosols and radiative forcing from GHGs; the fourth PC is dominated by compensation between the ventilation timescales of different ocean fractions. (PC5 is similarly ocean-dominated; see Figure S5.)



Altogether these PCA results suggest that the observational constraints used herein collapse the 25 model parameters around a four-dimensional subspace, and that these four dimensions reflect the balance between the effects of climate feedbacks, greenhouse gases, and aerosols on atmospheric and oceanic warming, as well as the structure of the large-scale ocean circulation.

Note also there are numerous ways to quantify the number of interpretable or meaningful PCs resulting from a PCA (Jackson, 1993); the first four PCs we focus on here only explain 30.1% of the total variance in the dataset, but the decisive break in the scree plot (fig. 6a) indicates strong evidence that these PCs are qualitatively different than the remaining PCs 5-25. We interpret the remaining variance in the data as reflective of the large amount of parametric uncertainty left in these models beyond what the observations herein can constrain, attesting to the importance of large ensemble simulations as employed here for quantifying uncertainty in ECS and TCR.

#### 4.2.3 Stepwise regression

It is also of interest to what extent the model outputs are directly predictable from or explicable by the individual model parameters and/or PCs. Given the roughly Gaussian and linear model equations, multilinear regression is a suitable approach to identifying these links; in particular stepwise regression (Draper & Smith, 1981) follows an automatic procedure of including and removing explanatory variables from the model fit to identify an optimal combination. We perform stepwise regression to predict the model outputs from the model parameters and/or the first , (de)selecting explanatory variables using the Bayesian Information Criterion (Schwartz, 1978) and also including interactions between model parameters (i.e. their products).

We find  $ECS_{100}$  to be significantly a function of all of PC1-4 and their interactions, with an  $R^2 = 0.24$ . Including only PC1-3 only reduces  $R^2$  by 0.0019, i.e.  $R^2 = 0.24$  still. While this is not an especially good fit, it is 98.1% of the variance in the model parameters explained by these PCs (24.2%), i.e. almost all of the model parameter variance these PCs explain directly translates to explained variance in  $ECS_{100}$ . In combination with the PCA results, this suggests the observations used here collapse the model parameters around four degrees of freedom, and that  $ECS_{100}$  is proportional to these first three degrees of freedom and their interactions, with the remaining variance in  $ECS_{100}$  due to the remaining variance in the model parameters. This implies that the observational constraints used here directly constrain  $ECS_{100}$  in our modeling approach, with very little information lost through constraining model parameters. In contrast, other model outputs (e.g.  $ECS_{20}$  or the whole-ocean carbon content) are poorly predicted by these PCs ( $R^2 = 0.10$  or less).

We also performed stepwise regression of model outputs against the 25 model parameters. We found  $ECS_{100}$  to be a significant function of only seven model parameters ( $R^2 = 0.40$ ; the three feedbacks  $\lambda$ , the whole-ocean to sea-surface



warming ratio  $r_2$ , the aerosol forcing coefficients  $\gamma_{NH_3}$  and  $\gamma_{ENMVOC}$ , and the  $CO_2$  forcing coefficient  $a_{CO_2}$ ).  $ECS_{20}$  by contrast was not a significant function of  $\gamma_{NH_3}$  or  $r_2$  but was a significant function of the slow feedback timescale  $\tau_{slow}$  (as well as the  $\lambda_s$  and  $a_{CO_2}$ ;  $R^2 = 0.40$ ). This implies both that ECS is not strongly dependent on the other parameters in the model used here, and also that there is a large amount of variation in ECS that can be reduced by better constraining these parameters. In contrast, other model outputs are sensitive to more model parameters and also more predictable; for instance the whole-ocean carbon content increase from 1982-2018 ( $\Delta C$ ) is a significant function of 20 model parameters ( $R^2 = 0.97$ ). For this latter case, these various dependencies can be simplified to some extent into a single parameter, the fraction of the ocean which is ventilated over a given timescale  $V_{vent,t}$ , which is a function of the different ocean boxes' volumes and exchange timescales (see Supplementary Information); on the intermediate 50-year timescale  $V_{vent,50}$  alone explains 75% of the variance in  $\Delta C$ . This is likely due to the simple carbon cycle in the model, whereas a more complex representation of the carbon cycle model would have numerous dependencies not considered here that would decrease the relative importance of  $V_{vent,t}$  in determining  $\Delta C$ . Surprisingly,  $V_{vent,t}$  is not a notably good predictor of other properties of interest (ECS, OHC) and when included in the aforementioned analyses in this section does not meaningfully affect the results or their interpretation.

330

## 5. Discussion

Many studies have combined reconstructions of surface temperature and ocean heat uptake with estimates of radiative forcing to calculate the effective climate feedback during the historic period (e.g. Annan, 2015; Anan and Hargreaves, 2020; Bodman and Jones, 2016; Lewis and Curry, 2014; Skeie et al., 2018; Otto et al., 2013; Tokarska et al., 2020). However, climate feedback strengths evolve over time in complex climate models (e.g. Andrews et al., 2015), indicating that effective climate sensitivity values obtained from historic observations may not apply into the future.

335

This study applies the historic observational record to constrain how effective climate sensitivity evolves on different response timescales (Figs. 3,4), utilising a model of independent climate feedback terms that respond to forcing over instantaneous (Planck), fast (several days) and slow (multi-decadal) timescales (eqns. 2,3,4). A Bayesian approach is adopted, where uniform prior probability distributions are applied for the fast and slow climate feedbacks (Fig. 2, Supplementary Table S1). Different temperature and ocean heat content observational datasets (Supplementary Table S2, eqns. 6,7,8) are applied to extract posterior probability distributions (Figs. 2). We then use these posterior probability distributions to evaluate effective climate sensitivity (ECS) and transient climate response (TCR) from  $4xCO_2$  and  $1pctCO_2$  forcing scenarios respectively.

345

Our estimates of ECS on a 20-year timescale is directly comparable to estimates of climate sensitivity made from historical constraints (e.g. Otto et al., 2013; Lewis and Curry, 2014), without explicitly considering the impact of additional slow climate feedbacks that may not have had time to equilibrate in the present day.



350

Our estimates of ECS on a 100-year timescale is directly comparable to the climate sensitivity estimates evaluated in complex climate model simulations from simulations lasting order 100 years, for example using the Gregory et al. (2004) method, and directly comparable to estimates of climate sensitivity from the palaeo-record where any longer, 1000-year, Earth system sensitivity feedbacks have been eliminated (e.g. Rohling et al., 2012; 2018).

355

We find that the differences in temperature and heat content datasets have a significant impact on the implied probability distributions of ECS (Figs. 1,3,4; Table 1). However, the implied probability distributions for TCR are sensitive to differences in temperature datasets but not to the differences in ocean heat content datasets (Figs. 1,5; Table 1).

360

The Cowtan&Way (Cowtan and Way, 2014) temperature reconstruction implies a larger ECS and TCR than HadCRUT4 (Figs. 3,4,5; Table 1), because the additional recent warming in Cowtan&Way (Fig. 1a) implies more positive slow climate feedbacks (Fig. 2). The Cheng et al. (2017) ocean heat content reconstruction implies larger ECS than the NODC reconstruction (Fig. 3,4; Table 1), because the additional ocean heat content uptake (Fig. 1b) in Cheng et al. (2017), with identical historic warming, must be balanced by a larger ECS (eq. 2). However, the different heat content datasets make almost no impact on TCR (Fig. 5; Table 1), possibly because larger historic heat content also implies larger heat uptake on a 1pctCO<sub>2</sub> scenario and this balances any warming impact of a larger ECS.

365

Our method constrains ECS over multiple response timescales (Fig. 3; Table 1). Our constraints on ECS over a 100-year response timescale (ECS<sub>100</sub>; Table 1) is directly comparable to previous reviews of climate sensitivity in the literature in AR5 (IPCC, 2013) and Sherwood et al. (2020). The IPCC (2013) AR5 estimate of ECS has a 66% range of 1.5 to 4.5 K (IPCC, 2013), while the recent Sherwood et al. (2020) Bayesian review has a narrower baseline 66% range of 2.6 to 3.6 K. The Sherwood et al. (2020) range removes both the lower portion of the IPCC ECS range (from 1.5 to 2.5 K) and the upper portion (from 3.7 to 4.5 K) at 66% confidence, suggesting a similar best estimate but with reduced uncertainty than IPCC (2013).

375

Our posterior 66% ranges for ECS<sub>100</sub> constrained by historical observations show a more complicated link to the IPCC (2013) range that depends on the combination of statistical interpretations of historic temperature and heat content observations used (Table 1). When applying the HadCRUT4 temperature and NODC heat content datasets, our method provides a 66% range on ECS<sub>100</sub> of 1.7 to 3.2 K, in agreement with the lower portion of the IPCC (2013) range. However, when the Cowtan&Way temperature and Cheng et al. heat content datasets are used our method supports the upper end of the IPCC (2013) range, from 2.3 to 4.2 K (Table 1; Figure 3). Therefore, we find that historical observations of temperature and ocean heat content support the IPCC (2013) range for Equilibrium Climate Sensitivity, but that different statistical interpretations of how historical observations produce global mean changes support different portions of the IPCC (2013)

380



385 ECS range. This finding demonstrates how differences in the statistical interpretations of global mean surface temperature and global ocean heat content changes from underlying observations lead to different implications for climate sensitivity and future warming.

**Code availability:** The WASP model code used here is available for download at <http://doi.org/10.5281/zenodo.4088074>.

390 **Data availability:** The datasets used (Supplementary Table S2) are publicly available: HadCRUT4 is available at <https://www.metoffice.gov.uk/hadobs/hadcrut4/data/current/download.html>. Cowtan and Way v2 ‘HadCRUT4 infilled by kriging’ is available at [https://www-users.york.ac.uk/~kdc3/papers/coverage2013/had4\\_krig\\_annual\\_v2\\_0\\_0.txt](https://www-users.york.ac.uk/~kdc3/papers/coverage2013/had4_krig_annual_v2_0_0.txt); NODC is available at [https://www.nodc.noaa.gov/OC5/3M\\_HEAT\\_CONTENT/](https://www.nodc.noaa.gov/OC5/3M_HEAT_CONTENT/). Cheng et al. is available at [http://159.226.119.60/cheng/images\\_files/IAP\\_OHC\\_estimate\\_update.txt](http://159.226.119.60/cheng/images_files/IAP_OHC_estimate_update.txt). HadSST3 is available at <https://www.metoffice.gov.uk/hadobs/hadsst3/data/download.html>. The Global Carbon Budget 2018 data is available at <https://doi.org/10.18160/gcp-2018>.

**Author contribution:** PG and BBC conceived the experiments. PG conducted the WASP model ensembles. PC and BBC analysed model output and wrote the manuscript.

400 **Competing interests:** The authors declare that they have no conflict of interest.

## Acknowledgements

PG acknowledges support from UKRI Natural Environmental Research Council grant NE/T010657/1. PG acknowledges support from the University of Southampton IRIDIS4 computing cluster, which was used to perform the WASP climate model ensembles. BBC acknowledges support from the National Environmental Research Council (NE/315R015953/1) and the Horizon 2020 Framework Programme (820989, project COMFORT). The work reflects only the authors’ view; the European Commission and their executive agency are not responsible for any use that may be made of the information the work contains.

## References

410 Andrews T., Gregory J.M., Webb M.J.: The dependence of radiative forcing and feedback on evolving patterns of surface temperature change in climate models. J Clim 28:1630–1648. <https://doi.org/10.1175/JCLI-D-14-00545.1>, 2015.



- 415 Annan, J.D.: Recent Developments in Bayesian Estimation of Climate Sensitivity. *Current Climate Change Reports*, 1, 263-267, <https://doi.org/10.1007/s40641-015-0023-5>, 2015.
- Annan, J. D., Hargreaves, J. C.: Bayesian deconstruction of climate sensitivity estimates using simple models: implicit priors and the confusion of the inverse, *Earth Syst. Dynam.*, 11, 347–356, <https://doi.org/10.5194/esd-11-347-2020>, 2020
- 420 Bodman, R.W., Jones, R.N.: Bayesian estimation of climate sensitivity using observationally constrained simple climate models. *WIREs Climate Change*, 7, 461–473. <https://doi.org/10.1002/wcc.397>, 2016.
- Cattell, R.B.: The scree test for the number of factors. *Journal of Multivariate Behavioral Research* 1, 245-276, 1966.
- 425 Cheng, L., Trenberth, K.E., Fasullo, J., Boyer, T., Abraham, J., Zhu, J.: Improved estimates of ocean heat content from 1960 to 2015. *Science Advances*, 3, 3, e1601545, <https://doi.org/10.1126/sciadv.1601545>, 2017.
- Cowan, K., Way, R.G.: Coverage bias in the HadCRUT4 temperature series and its impact on recent temperature trends. *Q. J. R. Meteorol. Soc.* 140, 1935–1944, <https://doi.org/10.1002/qj.2297>, 2014.
- 430 Draper, N., Smith, H.: *Applied Regression Analysis*, 2nd Edition, New York: John Wiley & Sons, Inc., 1981.
- Etminan, M., Myhre, G., Highwood, E.J., Shine, K.P.: Radiative forcing of carbon dioxide, methane, and nitrous oxide: A significant revision of the methane radiative forcing, *Geophys. Res. Lett.*, 43, 12,614–12,623, <https://doi:10.1002/2016GL071930>, 2016.
- 435 Goodwin, P.: On the time evolution of climate sensitivity and future warming, *Earth's Future* 6, EFT2466, <https://doi.org/10.1029/2018EF000889>, 2018.
- 440 Goodwin, P.: How historic simulation-observation discrepancy affects future warming projections in a very large model ensemble, *Climate Dynamics*, 47, 2219-2233, CLDY-D-15-00368R2, <https://doi.org/10.1007/s00382-015-2960-z>, 2016.
- Gregory, J.M., Andrews, T., Ceppi, P., Mauritsen, T., Webb, M.J.: How accurately can the climate sensitivity to CO<sub>2</sub> be estimated from historical climate change? *Climate Dynamics*, 54, 129-157, <https://doi.org/10.1007/s00382-019-04991-y>, 2019.
- 445



- Gregory, J.M., Andrews, T., Good, P., Mauritsen, T., Forster, P.M.: Small global-mean cooling due to volcanic radiative forcing. *Climate Dynamics*, 47, 3979-3991, <https://doi.org/10.1007/s00382-016-3055-1>, 2016.
- Gregory, J. M., Ingram, W.J., Palmer, M.A., Jones, G.S., Stott, P.A., Thorpe, R.B., Lowe, J.A., Johns, T.C., Williams, K.D.:  
450 A new method for diagnosing radiative forcing and climate sensitivity, *Geophys. Res. Lett.*, 31, L03205, <https://doi.org/10.1029/2003GL018747>, 2004.
- IPCC: Climate Change 2013: The Physical Science Basis. Contribution of Working Group 1 to the Fifth Assessment Report of the Intergovernmental Panel on Climate Change In T. F. Stocker, et al. (Eds.). (1535 pp.). Cambridge, UK: Cambridge  
455 University Press. <https://doi.org/10.1017/CBO9781107415324>, 2013.
- Jackson, D.A.: Stopping Rules in Principal Components Analysis: A Comparison of Heuristical and Statistical Approaches. *Ecology*, Vol. 74, No. 8, 2204-2214, 1993.
- 460 Jones, P. D., Harpham, C.: Estimation of the absolute surface air temperature of the Earth. *J. Geophys. Res. Atmos.*, 118, 3213–3217, <https://doi.org/10.1002/jgrd.50359>, 2013.
- Jolliffe, I.T.: Principal components in regression analysis. *Principal component analysis*. Springer, New York, NY, 129-155, 1986.
- 465 Kennedy J.J., Rayner, N.A., Smith, R.O., Saunby, M. and Parker, D.E.: Reassessing biases and other uncertainties in sea-surface temperature observations since 1850 part 1: measurement and sampling errors. *J. Geophys. Res.*, 116, D14103, <https://doi.org/10.1029/2010JD015218>, 2011.
- 470 Knutti, R., Rugenstein, M.A.A., Hegerl, G.C.: Beyond equilibrium climate sensitivity, *Nature Geoscience*, 10, 727-736, <https://doi.org/10.1038/NGEO3017>, 2017.
- le Quéré, C., Andrew, R. M., Friedlingstein, P., Sitch, S., Hauck, J., Pongratz, J., Pickers, P. A., Korsbakken, J. I., Peters, G. P., Canadell, J. G., Arneeth, A., Arora, V. K., Barbero, L., Bastos, A., Bopp, L., Chevallier, F., Chini, L. P., Ciais, P., Doney, S. C., Gkritzalis, T., Goll, D. S., Harris, I., Haverd, V., Hoffman, F. M., Hoppema, M., Houghton, R. A., Hurtt, G., Ilyina, T., Jain, A. K., Johannessen, T., Jones, C. D., Kato, E., Keeling, R. F., Goldewijk, K. K., Landschützer, P., Lefèvre, N., Lienert, S., Liu, Z., Lombardozi, D., Metzl, N., Munro, D. R., Nabel, J. E. M. S., Nakaoka, S., Neill, C., Olsen, A., Ono, T., Patra, P., Peregón, A., Peters, W., Peylin, P., Pfeil, B., Pierrot, D., Poulter, B., Rehder, G., Resplandy, L., Robertson, E., Rocher, M., Rödenbeck, C., Schuster, U., Schwinger, J., Séférian, R., Skjelvan, I., Steinhoff, T., Sutton, A., Tans, P. P., Tian, H.,



- 480 Tilbrook, B., Tubiello, F. N., van der Laan-Luijkx, I. T., van der Werf, G. R., Viovy, N., Walker, A. P., Wiltshire, A. J.,  
Wright, R., Zaehle, S., and Zheng, B.: Global Carbon Budget 2018, *Earth Syst. Sci. Data*, 10, 2141–2194,  
<https://doi.org/10.5194/essd-10-2141-2018>, 2018.
- Levitus, S., Antonov, J.I., Boyer, T.P., Baranova, O.K., Garcia, H.E., Locarnini, R.A., Mishonov, A.V., Reagan, J.R.,  
485 Seidov, D., Yarosh, E.S. and Zweng, M.M.: World ocean heat content and thermosteric sea levelchange (0–2000 m), 1955–  
2010. *Geophysical Research Letters*, 39, <https://doi.org/10.1029/2012GL051106>, 2012.
- Lewis, N., Curry, J.A.: The implications for climate sensitivity of AR5 forcing and heat uptake estimates. *Climate  
Dynamics*, 45, 1009–1023, <https://doi.org/10.1007/s00382-014-2342-y>, 2014.
- 490 Marvel, K., Schmidt, G.A., Miller, R.L., Nazarenko, L.S.: Implications for climate sensitivity from the response to individual  
forcings. *Nature Climate Change*, 6, <https://doi.org/10.1038/nclimate2888>, 2015.
- Morice, C.P., Kennedy, J.J., Rayner, N.A. and Jones, P.D.: Quantifying uncertainties in global and regional temperature  
495 change using an ensemble of observational estimates: the HadCRUT4 dataset. *Journal of Geophysical Research*, 117,  
D08101, <https://doi.org/10.1029/2011JD017187>, 2012
- Myhre, G., Samset, B. H., Schulz, M., Balkanski, Y., Bauer, S., Bernsten, T. K., Bian, H., Bellouin, N., Chin, M., Diehl, T.,  
Easter, R. C., Feichter, J., Ghan, S. J., Hauglustaine, D., Iversen, T., Kinne, S., Kirkevåg, A., Lamarque, J.-F., Lin, G., Liu,  
500 X., Lund, M. T., Luo, G., Ma, X., van Noije, T., Penner, J. E., Rasch, P. J., Ruiz, A., Seland, Ø., Skeie, R. B., Stier, P.,  
Takemura, T., Tsigaridis, K., Wang, P., Wang, Z., Xu, L., Yu, H., Yu, F., Yoon, J.-H., Zhang, K., Zhang, H., and Zhou, C.:  
Radiative forcing of the direct aerosol effect from AeroCom Phase II simulations, *Atmos. Chem. Phys.*, 13, 1853–1877,  
<https://doi.org/10.5194/acp-13-1853-2013>, 2013.
- 505 Nicholls, Z.R.J., Meinshausen, M., Lewis, J., Gieseke, R., Dommenges, D., Dorheim, K., Fan, C.-S., Fuglestedt, J.S.,  
Gasser, T., Golüke, U., Goodwin, P., Kriegler, E., Leach, N.J., Marchegiani, D., Quilcaille, Y., Samset, B.H., Sandstad, M.,  
Shiklomanov, A.N., Skeie, R.B., Smith, C.J., Tanaka, K., Tsutsui, J., Xie, Z.: Reduced complexity model intercomparison  
project phase 1: Protocol, results and initial observations. *Geoscientific Model Development*. 2020 in press
- 510 O'Neill, B. C., Tebaldi, C., van Vuuren, D. P., Eyring, V., Friedlingstein, P., Hurtt, G., Knutti, R., Kriegler, E., Lamarque, J.-  
F., Lowe, J., Meehl, G. A., Moss, R., Riahi, K., and Sanderson, B. M.: The Scenario Model Intercomparison Project  
(ScenarioMIP) for CMIP6, *Geosci. Model Dev.*, 9, 3461–3482, <https://doi.org/10.5194/gmd-9-3461-2016>, 2016.



515 Otto, A., Otto, F.E.L., Boucher, O., Church, J., Hegerl, G., Forster, P.M., Gillet, N.P., Gregory, J., Johnson, G.C., Knutti, R.,  
Lewis, N., Lohmann, U., Marotzke, J., Myhre, G., Shindell, D., Stevens, B., Allen, M.R.: Energy budget constraints on  
climate response. *Nature Geoscience*, 6, 415–416, <https://doi.org/10.1038/ngeo1836>, 2013.

Proistosescu, C., and Huybers, P.J.: Slow climate mode reconciles historical and model-based estimates of climate  
sensitivity, *Science Advances*, 3, <https://doi.org/10.1126/sciadv.1602821>, 2017.

520

Rohling, E.J., Sluijs, A., Dijkstra, H. A., Köhler, P., van de Wal, R.S.W., von der Heydt, A. S., Beerling, D.J., Berger, A.,  
Bijl, P.K., Crucifix, M., DeConto, R., Drijfhout, S.S., Fedorov, A., Foster, G.L., Ganopolski, A., Hansen, J., Hönlisch, B.,  
Hooghiemstra, H., Huber, M., Huybers, P., Knutti, R., Lea, D.W., Lourens, L.J., Lunt, D., Masson-Delmotte, V., Medina-  
Elizalde, M., Otto-Bliesner, B., Pagani, M., Pälike, H., Renssen, H., Royer, D.L., Siddall, M., Valdes, P., Zachos J.C.,  
525 Zeebe, R. E.: Making sense of palaeoclimate sensitivity. *Nature*, 491, 683–691, <https://doi.org/10.1038/nature11574>, 2012.

Rohling, E.J., Marino, G., Foster, G.L., Goodwin, P.A., von der Heydt, A.S., Köhler, P.: Comparing climate sensitivity,  
past and present. *Annual Review of Marine Science*, 10, 261–288, <https://doi.org/10.1146/annurev-marine-121916-063242>,  
2018.

530

Rugenstein, M., Bloch-Johnson, J., Gregory, J., Andrews, T., Mauritsen, T., Li, C., Frölicher, T.L., Paynter, D., Gokhan  
Danabasoglu, G., Yang, S., Dufresne, J.-L., Cao, L., Schmidt, G.A., Abe-Ouchi, A., Geoffroy, O., Knutti, R.: Equilibrium  
climate sensitivity estimated by equilibrating climate models. *Geophysical Research Letters*, 47, e2019GL083898.  
<https://doi.org/10.1029/2019GL083898>, 2020.

535

Schwarz, G.E.: Estimating the dimension of a model. *Annals of Statistics*, 6 (2): 461–464, 1978.

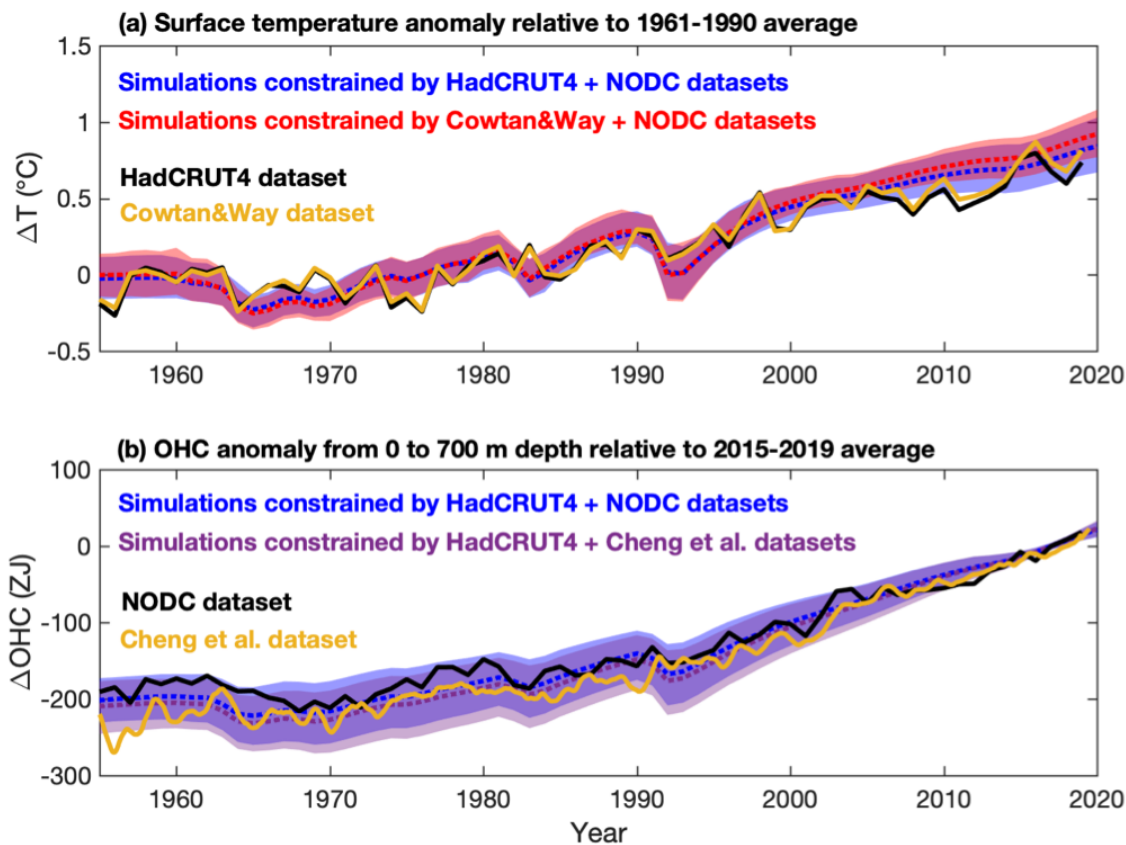
Senior, C., Mitchell, J. F.: The time-dependence of climate sensitivity. *Geophysical Research Letters*, 27(17), 2685–2688.  
<https://doi.org/10.1029/2000GL011373>, 2000.

540

Sherwood, S., Webb, M.J., Annan, J.D., Armour, K.C., Forster, P.M., Hargreaves, J.C., Hegerl, G., Klein, S.A., Marvel,  
K.D., Rohling, E.J., Watanabe, M., Andrews, T., Braconnot, P., Bretherton, C.S., Foster, G.L., Hausfather, Z., von der  
Heydt, A.S., Knutti, R., Mauritsen, T., Norris, J.R., Proistosescu, C., Rugenstein, M., Schmidt, G.A., Tokarska, K.B., Zelinka,  
M.D.: An assessment of Earth’s climate sensitivity using multiple lines of evidence. *Reviews of Geophysics*, 58,  
545 <https://doi.org/10.1029/2019RG000678>, 2020.



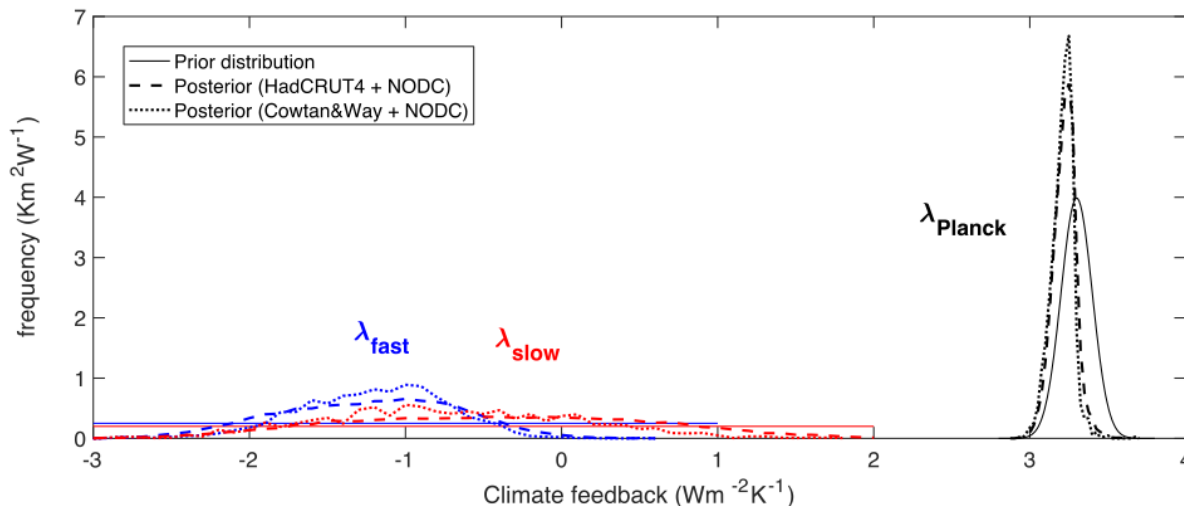
- Skeie, R.B., Berntsen, T., Aldrin, M., Holden, M., and Myhre, G.: Climate sensitivity estimates – sensitivity to radiative forcing time series and observational data. *Earth System Dynamics*, 9, 879-894, <https://doi.org/10.5194/esd-9-879-2018>, 2018.
- 550
- Smith, C.J., Forster, P.M., Allen, M., Leach, N., Millar, R.J., Passerello, G.A., and Regayre, L.A.: FAIR v1.3: a simple emissions-based impulse response and carbon cycle model. *Geoscientific Model Development*, 11, 2273-2297, <https://doi.org/10.5194/gmd-11-2273-2018>, 2018.
- 555 Tokarska, K.B., Hegerl, G.C., Schurer, A.P., Forster, P.M., and Marvel, K.: Observational constraints on effective climate sensitivity from the historical period, *Environmental Research Letters*, 15, 3, <https://doi.org/10.1088/1748-9326/ab738f>, 2020.
- Trenberth, K.E., Fasullo, J.T., and Balmaseda, M.A.: Earth's Energy Imbalance, *Journal of Climate*, 27, 3129-3144.
- 560 <https://doi.org/10.1175/JCLI-D-13-00294.1>, 2014.
- van der Ent, R. J., Tuinenburg, O. A.: The residence time of water in the atmosphere revisited. *Hydrology and Earth System Sciences*, 21, 779–790. <https://doi.org/10.5194/hess-21-779-2017>, 2017.



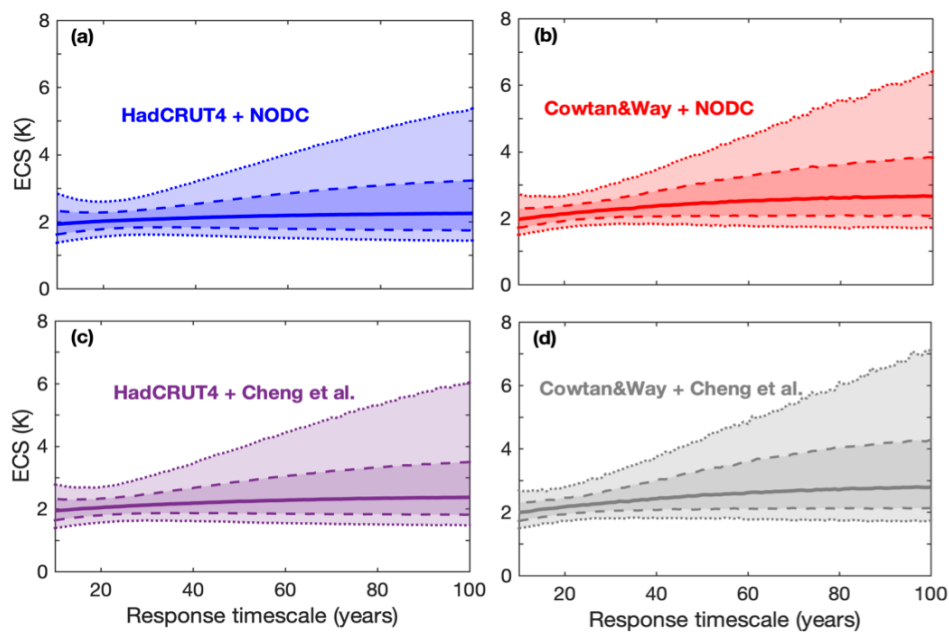
565

570

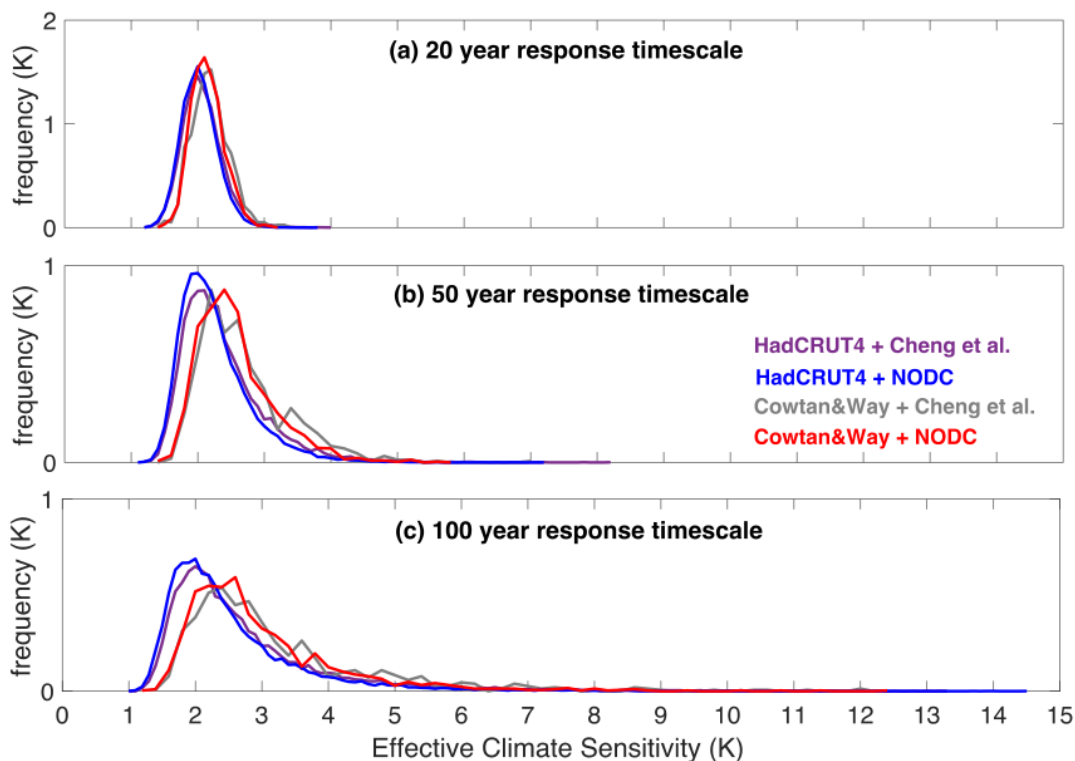
Figure 1. Surface temperature and ocean heat content anomalies from 1955 from datasets and dataset-constrained simulations. (a) Historic surface warming relative to the 1961-1990 average in the HadCRUT4 and Cowtan&Way surface temperature datasets (solid lines) and posterior ensemble simulations (dotted lines show ensemble medians, shading show 95% ensemble ranges) constrained by each temperature dataset along with the NODC ocean heat content dataset. (b) Ocean Heat Content (OHC) anomaly in the upper 700m of the global ocean in the NODC and Cheng et al. datasets (solid lines) and posterior ensemble simulations (dotted lines show ensemble medians, shading show 95% ensemble ranges) constrained by each OHC dataset along with the HadCRUT4 temperature dataset.



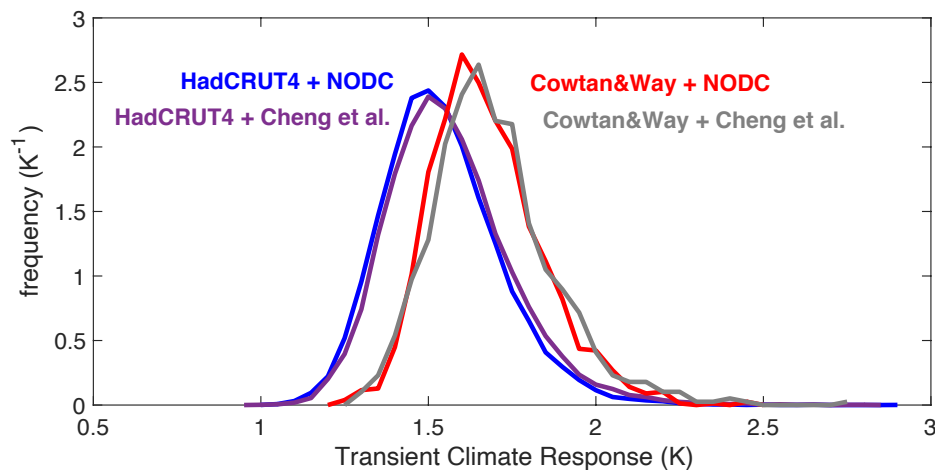
575 **Figure 2: Prior and posterior probability densities for the Planck climate feedback (black), fast climate feedback (blue) and slow climate feedback (red). The prior distributions (thin solid lines) and posterior distributions when constrained by HadCRUT4 + NODC datasets (dashed lines) and Cowtan&Way + NODC datasets (dotted lines) are shown.**



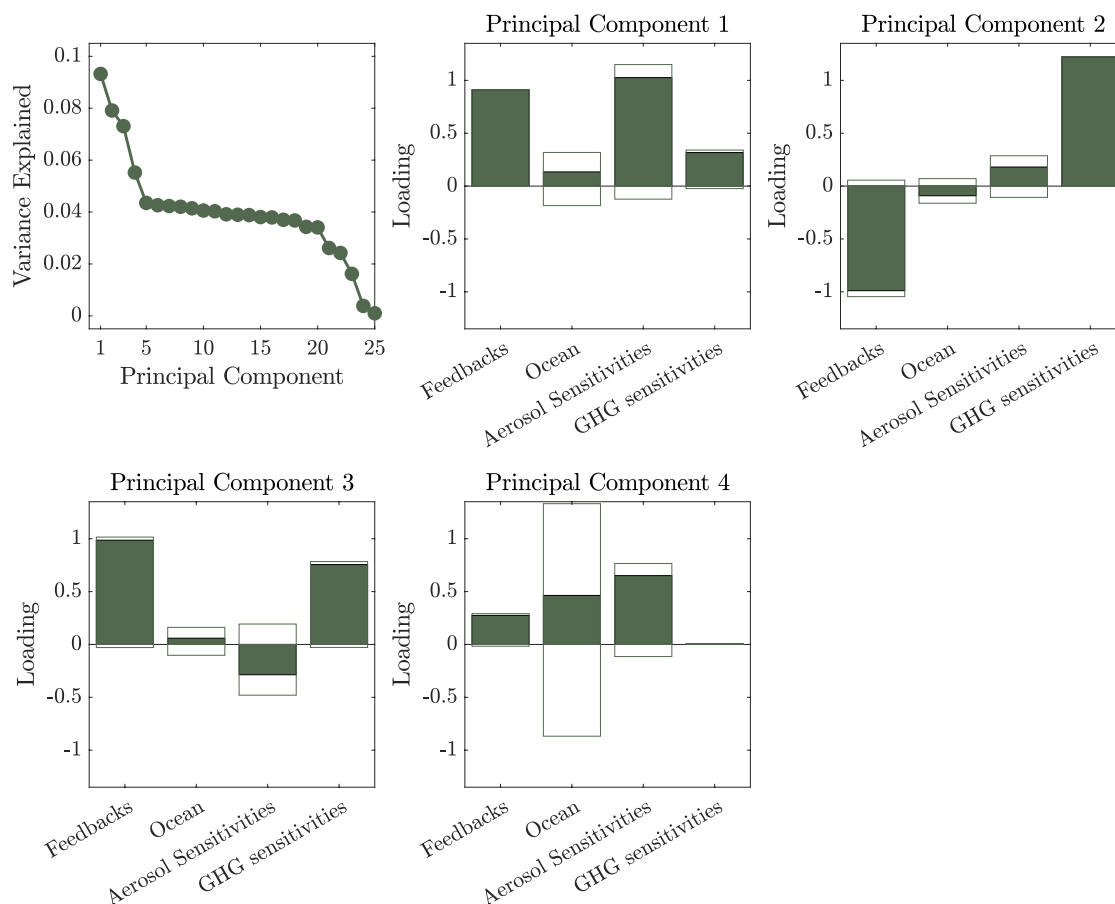
580 **Figure 3: Effective Climate Sensitivity (ECS) from 10 to 100-year response timescales following a 4xCO<sub>2</sub> forcing scenario constrained by different combinations of observational reconstructions. Solid line is median, dashed line and dark shading is 66% range and dotted lines and light shading is 95% range.**



585 **Figure 4: Probabilistic estimates of Effective Climate Sensitivity for different combinations of observational constraints over (a) a 20-year response timescale, (b) a 50-year response timescale and (c) a 100-year response timescale. When constrained by the HadCRUT4 temperature record the most likely (modal) ECS value is ~2.0 K on all timescales. For the Cowtan&Way temperature record the most likely ECS value is ~2.1 K on 20-year timescale rising to ~2.5 K on longer 50-year and 100-year timescales.**



590 **Figure 5: Transient Climate Response (TCR) for combinations of temperature and heat content datasets, evaluated from 1pctCO2 scenario using the 11-year average warming centred on the moment of CO2 doubling.**



595 **Figure 6: Principle Component Analysis of the posterior model ensembles. a) Scree plot of PC vs. variance explained. b-e) PCs**  
**simplified into climate feedbacks and their response timescales (*Feedbacks*); parameters describing ocean circulation and ocean**  
**heat and carbon transport (*Ocean*); the sensitivity of radiative forcing to aerosols (*Aerosol sensitivities*) and the sensitivity of**  
**radiative forcing to Green House Gasses (*GHG sensitivities*)). White parts of the bar plots show the total positive and total negative**  
 600 **contributions, green parts of bar plots show the sum of positive and negative contributions. PC1 reflects a how climate feedback**  
**and aerosol radiative forcing co-vary in the posterior ensemble, while PC2 reflects co-variation between climate feedback and**  
**GHG radiative forcing. PC3 reflects how climate feedbacks vary with both aerosol radiative forcing and GHG radiative forcing in**  
**the posterior ensemble. PC4 reflects how ocean circulation, heat and carbon uptake vary with aerosol forcing and climate**  
**feedback.**

605

610



Dataset combination	ECS on 20-year timescale (K)	ECS on 50-year timescale (K)	ECS on 100-year timescale (K)	TCR (K)
HadCRUT4 + NODC	Median: 2.0 66% CI: 1.8 to 2.3 90% CI: 1.6 to 2.5 95% CI: 1.5 to 2.6	Median: 2.2 66% CI: 1.8 to 2.7 90% CI: 1.6 to 3.3 95% CI: 1.5 to 3.6	Median: 2.2 66% CI: 1.7 to 3.2 90% CI: 1.5 to 4.5 95% CI: 1.4 to 5.4	Median: 1.5 66% CI: 1.4 to 1.7 90% CI: 1.3 to 1.9 95% CI: 1.2 to 1.9
HadCRUT4 + Cheng et al.	Median: 2.0 66% CI: 1.8 to 2.3 90% CI: 1.6 to 2.6 95% CI: 1.6 to 2.7	Median: 2.2 66% CI: 1.8 to 2.9 90% CI: 1.6 to 3.5 95% CI: 1.6 to 4.0	Median: 2.4 66% CI: 1.8 to 3.5 90% CI: 1.6 to 5.0 95% CI: 1.5 to 6.0	Median: 1.5 66% CI: 1.4 to 1.7 90% CI: 1.3 to 1.9 95% CI: 1.3 to 2.0
Cowtan&Way + NODC	Median: 2.1 66% CI: 1.9 to 2.4 90% CI: 1.8 to 2.6 95% CI: 1.7 to 2.7	Median: 2.5 66% CI: 2.1 to 3.0 90% CI: 1.9 to 3.6 95% CI: 1.8 to 3.9	Median: 2.7 66% CI: 2.1 to 3.8 90% CI: 1.8 to 5.4 95% CI: 1.7 to 6.4	Median: 1.7 66% CI: 1.5 to 1.8 90% CI: 1.4 to 2.0 95% CI: 1.4 to 2.0
Cowtan&Way + Cheng et al.	Median: 2.2 66% CI: 1.9 to 2.4 90% CI: 1.8 to 2.7 95% CI: 1.7 to 2.8	Median: 2.5 66% CI: 2.1 to 3.3 90% CI: 1.9 to 4.0 95% CI: 1.8 to 4.3	Median: 2.8 66% CI: 2.1 to 4.3 90% CI: 1.8 to 6.1 95% CI: 1.7 to 7.1	Median: 1.7 66% CI: 1.5 to 1.9 90% CI: 1.4 to 2.0 95% CI: 1.4 to 2.1

615 **Table 1: Effective Climate Sensitivity (ECS, K) and Transient Climate Response (TCR, K) best estimate (median) and ranges (66%, 90% and 95% Confidence Intervals) under different observational constraints for surface warming and heat uptake.**